Am J Cancer Res 2022;12(8):3625-3643
www.ajcr.us /ISSN:2156-6976/ajcr0143393

Original Article

Brachyury promotes proliferation and migration of hepatocellular carcinoma via facilitating the transcription of NCAPG2

Song Li[1*], Yijie Lu[1*], Yaopeng Xu[1], Cong Zhang[1], Biren Liu[1], Ancheng Qin[1], Zhiming Qiao[1], Cong Shen[2], Jun Shen[3], Yuting Liang[4], Jianwu Wu[1], Xinwei Jiang[1]

[1]Department of Hepatobiliary Surgery, Suzhou Municipal Hospital, The Affiliated Suzhou Hospital of Nanjing Medical University, Gusu School, Nanjing Medical University, Suzhou 215002, China; [2]State Key Laboratory of Reproductive Medicine, Nanjing Medical University, Nanjing 211166, China; [3]Department of Orthopeadic Surgery, Suzhou Municipal Hospital, The Affiliated Suzhou Hospital of Nanjing Medical University, Gusu School, Nanjing Medical University, Suzhou 215002, China; [4]Center for Clinical Laboratory, The First Affiliated Hospital of Soochow University, Suzhou 215006, China. [*]Equal contributors.

Received April 8, 2022; Accepted July 13, 2022; Epub August 15, 2022; Published August 30, 2022

Abstract: Hepatocellular carcinoma (HCC) has a poor prognosis because of its limited drug responses in clinical trials. Therefore, it is crucial to clarify the molecular mechanisms of HCC progression to identify new diagnostic markers and therapeutic targets. Here, we report that brachyury, which regulates the gene encoding the non-SMC condensin II complex subunit G2 (NCAPG2), promotes tumorigenesis in HCC. Knockdown of brachyury led to inhibition of cancer progression *in vitro* and *in vivo*. Chromatin immunoprecipitation-sequencing data indicated that the oncogene NCAPG2 is a direct target of brachyury. Furthermore, NCAPG2 knockdown inhibited the proliferation and migration of HCC cells and attenuated brachyury-induced tumorigenesis. Overexpression and decreased DNA methylation of NCAPG2 were associated with a poor prognosis, and NCAPG2 was positively correlated with various immune cell infiltrates, cancer-associated fibroblasts, and immune checkpoint molecule expression levels in the tumor microenvironment. Moreover, the effectiveness of immune checkpoint blockade was decreased in the high NCAPG2 expression group. Together, these findings demonstrated a coregulatory effect of the brachyury/NCAPG2 axis during HCC progression.

Keywords: Hepatocellular carcinoma, brachyury, NCAPG2, tumorigenesis, tumor microenvironment

Introduction

According to the Global Cancer Statistics 2020 report [1], primary liver cancer is the sixth most commonly diagnosed cancer and the third leading cause of cancer death worldwide [1, 2]. Pathologically, hepatocellular carcinoma (HCC) is a major type of primary liver cancer [3]. Early diagnosis of HCC is difficult, and patients have a poor prognosis because medical treatments are limited. In addition, the 5-year recurrence rate of HCC patients is approximately 80%, even with timely surgical operation [4, 5]. Therefore, it is crucial to clarify the molecular mechanisms of HCC progression and identify new diagnostic markers and therapeutic targets.

Brachyury belongs to the T-box transcription factor family [6, 7], which shares a highly-conserved, sequence-specific DNA-binding domain of 180 to 200 amino acids known as the T-domain. Brachyury was initially reported to play a central role in notochord [8] and mesoderm specification [9]. Further studies from our group and others have found that brachyury is abnormally regulated in breast [10, 11], lung [12], prostate [13], testicular [14], and colorectal cancer [15] and other solid tumors, and abnormal regulation of brachyury is associated with the degree of malignancy and a poor prognosis. In particular, brachyury expression is elevated in tumor tissues compared with adjacent non-tumorous tissues, and it is closely related to distant metastasis and a poor prog-

nosis of liver cancer [16]. Overexpression of brachyury promotes the epithelial-mesenchymal transition (EMT) and metastasis of HCC cells in *vitro* and in *vivo* [16]. However, whether brachyury affects HCC cell proliferation and the underlying specific mechanisms remain unclear.

Non-SMC condensin II complex subunit G2 (NCAPG2) is a component of the chromosome condensin II complex, which is essential for chromosome condensation and segregation during mitosis [17]. NCAPG2 is upregulated in HCC, and it enhances HCC cell proliferation by inducing EMT and activating the STAT3 and NF-κB signaling pathways [18]. A previous study reported that NCAPG2 promotes HCC cell proliferation by acting as a direct downstream target of miR-375 [19]. These studies suggest that upregulation of NCAPG2 expression is closely related to HCC cell proliferation, and multiple mechanisms affect the ability of NCAPG2 to promote malignancy in HCC.

Here, to determine the precise function of brachyury in HCC, we systematically examined the carcinogenic effect of brachyury *in vitro* and *in vivo*. We reanalyzed the DNA regions with which the transcriptional factor brachyury interacts according to previously published chromatin immunoprecipitation-sequencing (ChIP-seq) data [10], and we used quantitative real-time polymerase chain reaction (qRT-PCR) assays to examine 60 potential target molecules whose expression is regulated by brachyury in two HCC cell lines. We investigated the role of NCAPG2, a direct target of brachyury, during HCC progression. In addition, we evaluated NCAPG2 expression as well as its correlation with HCC prognosis using three databases, including The Cancer Genome Atlas (TCGA), Genotype-Tissue Expression (GTEx), and Gene Expression Omnibus (GEO). We also examined the immune cell infiltration, immune checkpoint molecules, NCAPG2 methylation, stemness index, and pathway enrichment analysis data associated with NCAPG2, further confirming its carcinogenic role as an oncogene in HCC. The present findings suggested that candidate target genes of brachyury, including NCAPG2, are potential therapeutic targets in HCC associated with abnormal brachyury expression.

Materials and methods

Cell culture

The HepG2 and Huh7 human HCC cell lines were purchased from Zhong Qiao Xin Zhou Biotechnology Company (Shanghai, China). HepG2 cells were maintained in Minimum Essential Medium (MEM, Gibco Life Technologies, USA) supplemented with 10% fetal bovine serum (ExCell Bio, New Zealand), 1% penicillin/streptomycin (Invitrogen, Carlsbad, CA, USA), 1% sodium pyruvate (Thermo Fisher Scientific, Waltham, MA, USA), and 1% MEM Non-Essential Amino Acids Solution (Thermo Fisher Scientific). Huh7 cells were maintained in Dulbecco's modified Eagle medium (Thermo Fisher Scientific) supplemented with 10% fetal bovine serum (ExCell Bio) and 1% penicillin/streptomycin (Invitrogen). Both cell lines were cultured at 37°C in a humidified incubator containing 5% CO_2.

Cell transfection

To construct the brachyury overexpression plasmid, human brachyury cDNA was amplified by PCR and then cloned into the pcDNA3.0 vector (Invitrogen). To construct pGL6-NCAPG2 plasmids, both full length (-2000 - +1000 relative to the transcriptional start site) and partial (promoter-mut) NCAPG2 promoter sequences were amplified by PCR from human genomic DNA and inserted into the pGL6 firefly luciferase reporter vector (Beyotime, Nantong, China). The NCAPG2 promoter-mut construct was generated using the ClonExpress Ultra One Step Cloning Kit (Vazyme, Nanjing, China).

Small interfering RNA (siRNA) sequences targeting brachyury and NCAPG2 were purchased from GenePharma (Shanghai, China). Brachyury, NCAPG2, and negative control siRNAs were transfected into HepG2 and Huh7 cells using Lipofectamine 2000 (Invitrogen) according to the manufacturer's instructions. Cells were harvested for further analysis at 48 h post-transfection. The siRNA sequences were as follows: si-Brachyury#1, 5'-GCUGAACUCCUUGCAUAAG-3'; si-Brachyury#2, 5'-GGAUGUUUCCGGUGCUGAA-3'; si-NCAPG2#1, 5'-CAGCCUAAAUGAAUUACUA-3'; si-NCAPG2#2, 5'-GCGUAUCCAUCAAGCUUUA-3'; si-NCAPG2#3, 5'-GCCAAACUUUACACGAUUA-3'; and si-NC, 5'-UUCUCCGAACGUGUCACGU-3'.

Western blot analysis

Radioimmunoprecipitation assay buffer (Beyotime) supplemented with 1% (v/v) phenylmethanesulfonylfluoride (Beyotime) was used to extract total proteins from cells. Protein concentrations were analyzed using a bicinchoninic acid kit (Beyotime). Total proteins (30 μg) were electrophoresed by 10% sodium dodecyl sulfate-polyacrylamide gel electrophoresis and then transferred onto polyvinylidene difluoride membranes (Millipore, Billerica, MA, USA). After blocking with 5% nonfat milk, the membranes were incubated with the indicated primary antibodies (anti-brachyury and anti-GAPDH at 1:1000; Cell Signaling Technology, CST) overnight at 4°C. The membranes were then washed and incubated with horseradish peroxidase-conjugated secondary antibodies for 2 h at room temperature. The bands were visualized using an ECL Prime western blotting detection system. Anti-GAPDH was used in parallel as a loading control, and experiments were performed in triplicate.

RNA extraction and qRT-PCR

Total RNA was extracted with the TRIzol reagent (Invitrogen) according to the manufacturer's instructions. cDNA was synthesized from 1 μg of total RNA using a Prime Script Reverse Transcription Kit (Vazyme), as previously described [20, 21]. cDNA was used as the template for qRT-PCR using the ABI 7500 Real-Time PCR system (Applied Biosystems, Foster City, CA, USA) according to the manufacturer's instructions. The results were normalized to GAPDH expression and calculated based on the $2^{-\Delta\Delta CT}$ method. The following primers were used: NCAPG2-F, CTGTTCAGTCTCGGCACACA; NCAPG2-R, AACCTTCCGTAGCTGGTGAC; 18sRNA-F, AAACGGCTACCACATCCAAG; 18sRNA-R, CCTCCAATGGATCCTCGTTA; GAPDH-F, TGGCATTGCCCTCAACGAC; and GAPDH-R, TTTTCTGAGCCAGCCACCAGAG.

Cell viability assay

Cells were seeded in 96-well plates (3000 cells/well) and transfected once they reached approximately 70% confluence. After 48 h, cell viability was assessed every 24 h using a cell counting kit (CCK)-8 assay (Beyotime Biotechnology), as previously described [22, 23]. For the colony formation assay, cells were seeded in six-well plates (1000 cells/well) and cultured in complete medium containing 10% fetal bovine serum for 14 days. The medium was changed every 5 days. After 2 weeks, the cells were washed twice with phosphate-buffered saline (PBS) solution, fixed with methanol for 20 min, and stained with 0.1% crystal violet (Beyotime Biotechnology) for 20 min. The colonies were photographed and counted, and the process was performed in triplicate.

Cell migration assay

The cell migration capacity was evaluated via 24-well chambers with an 8-μm pore size, as previously described [24]. At 48 h post-transfection, HepG2 and Huh7 cells (3×10^4 cells) were resuspended in 300 μl of serum-free medium and placed in the upper chamber, and the lower chamber was filled with 700 μl of medium supplemented with 10% fetal bovine serum. After 48 h of culture, the cells on the upper membrane were removed with a sterile cotton swab, and the cells on the lower membrane surface were fixed with methanol for 20 min and stained with 0.1% crystal violet for 20 min. The cell number was counted under a microscope, and the experiment was performed in triplicate.

In vivo tumor growth assay

For the *in vivo* growth assay, 5-week-old athymic BALB/c nude mice were maintained under specific pathogen-free conditions. Huh7 cells transfected with short hairpin (sh)-brachyury or sh-negative control (NC) were washed twice with PBS and then digested with trypsin. Flank subcutaneous xenografts were then established by subcutaneous injection of 1×10^6 cells suspended in 200 μl of PBS. In each mouse, one side was injected with the treatment group, and the other side was injected with the control group. The tumor sizes were measured every 5 days. After 40 days, mice were sacrificed, and the subcutaneous tumors were removed. The tumor volumes and weights were evaluated, and the tumors were subjected to immunostaining with Ki67. All experimental protocols were approved by the Ethics Committee of Nanjing Medical University.

Immunofluorescence

Fresh subcutaneous tumor tissue was fixed with 4% paraformaldehyde for 48 h. The tissue was cut to an appropriate size with a scalpel and then dehydrated in a series of low-to-high concentrations of ethanol. The tissue was then

hyalinized with xylene, embedded in paraffin, sectioned at 6 μm, deparaffinized with xylene, and rehydrated in a series of low-to-high concentrations of ethanol, as previously reported [25, 26]. The antigen was retrieved in sodium citrate buffer (pH 6.0) for 20 min. The sections were then blocked with 5% bovine serum albumin and incubated with a primary antibody against Ki67 (Abcam) at 4°C overnight. After washing with PBS, the sections were incubated with secondary antibodies (Thermo Scientific), and cell nuclei were stained with 4',6-diamidino-2-phenylindole (DAPI, Beyotime Biotechnology). Samples were visualized using a Zeiss laser microscope (LSM800, Carl Zeiss, Oberkochen, Germany). The HCC tissue microarray was obtained from Zhongke Huaguang Biotech Co., Ltd. (Xi'an, China) and reacted with a primary antibody against brachyury (CST).

ChIP-qPCR assay

The ChIP-qPCR assay was performed using a ChIP assay kit (Millipore) with a standard protocol as previously reported [23, 27]. In brief, cells were harvested, washed, and cross-linked using 1% formaldehyde. The DNA-protein complexes were isolated and sheared into fragments of 300-500 bp. Isolated chromatin was immunoprecipitated using an anti-brachyury antibody and normal rabbit IgG (negative control). Immunoprecipitated DNA was analyzed by qRT-PCR using the following primers: human NCAPG2 forward, 5'-ATGATGGGGAGGAGGACACA-3'; and human NCAPG2 forward reverse, 5'-ACATAAACCCCCATTTGTGCAG-3'. The experiment was replicated three times.

Dual-luciferase reporter assay

Cells were cultured in 12-well plates and transiently transfected with 0.2 μg of the pGL6 luciferase reporter plasmid and brachyury effector plasmid. An internal control reporter plasmid containing Renilla luciferase (pRL-TK) was used for cotransfection to normalize the transfection efficiency. Two days after transfection, luciferase activity was detected using the Dual-luciferase Reporter Gene Assay System (Beyotime Biotechnology).

Dataset analyses

NCAPG2 expression data in cancer and normal tissues were obtained from the following databases: TCGA (https://portal.gdc.cancer.gov/), GTEx (https://gtexportal.org/), and GEO (GSE62232, GSE101685, and GSE112790 datasets).

Correlation analyses of NCAPG2 with tumor stage (such as the T stage), pathological stage, histological grade, and hepatitis B virus (HBV) infection were performed using data from TCGA and the ggplot package in R. Kaplan-Meier (KM) survival curve analyses were performed using the survival package in R. The cases were divided into high and low NCAPG2 expression groups based on the median expression level of NCAPG2. A log-rank test was performed to analyze the relationship between NCAPG2 expression and HCC survival outcomes, including overall survival (OS), progression-free survival (PFS), and disease-free survival (DFS).

The TIMER algorithm was used to analyze the correlations of NCAPG2 expression with immune cell infiltration and cancer-associated fibroblasts (CAFs) in HCC [28]. In addition, the correlations of NCAPG2 expression with macrophage M2 polarization and M2-like macrophage biomarkers were explored using quanTIseq algorithms. The association between NCAPG2 expression and tumor immune subtypes, including the wound healing (C1), interferon (IFN)-gamma dominant (C2), inflammatory (C3), lymphocyte depleted (C4), immunologically quiet (C5), and TGF-beta dominant (C6) subtypes, was analyzed using the TISDB website [29]. HCC is a representative inflammation-related cancer, and immune checkpoint inhibitors (ICIs) play an important role in its treatment [30]. The correlation of NCAPG2 expression with immune checkpoint molecule expression was evaluated using the ggplot2 package in R based on TCGA data. In addition, we predicted NCAPG2 gene expression using the TIDE algorithm to predict ICI responsiveness.

DNA methylation is an essential component of the epigenetic machinery that affects chromatin structure and regulates gene expression [31]. We assessed the DNA methylation sites of NCAPG2 using the MethSurv database (https://biit.cs.ut.ee/methsurv/). Moreover, KM survival analysis was performed to evaluate the relationship between DNA methylation sites of NCAPG2 and the OS of HCC patients.

Because cancer progression involves the gradual loss of a differentiated phenotype and

acquisition of progenitor and stem cell-like features [32], we assessed the tumor stemness score using the OCLR algorithm and analyzed the correlation between NCAPG2 expression and stemness scores in HCC patients.

To elucidate the signaling pathways that involve NCAPG2, we calculated the correlation between NCAPG2 and pathway scores using Spearman correlation coefficients in HCC patients in TCGA by gene set enrichment analysis (GSEA).

Statistical analysis

GraphPad Prism 8 software and R were used for the statistical analyses. Differences between groups were compared using the Wilcoxon rank-sum test, one-way analysis of variance, or a two-tailed Student's t-test as appropriate. Correlations were evaluated using Pearson or Spearman correlation coefficients as appropriate. KM plots were used to identify the significance of differences between survival outcomes, and differences with a value of $P < 0.05$, $P < 0.01$, $P < 0.001$, and $P < 0.0001$ were set as the thresholds for statistical significance.

Results

Brachyury knockdown suppresses HCC cell proliferation and migration in vitro

We first examined brachyury expression in HCC using a tissue microarray with 47 HCC and paired adjacent normal tissues. The immunostaining results revealed that brachyury was highly expressed in HCC tissues relative to paracancerous tissues (Figure S1).

To investigate the role of brachyury in HCC progression, we selected two HCC cell lines, HepG2 and Huh7, for functional verification. We performed brachyury siRNA knockdown experiments in both cell lines, and the siRNA sequences led to reduced brachyury protein expression compared with that in the control group (**Figure 1A**, **1B**). CCK8 assays demonstrated that brachyury knockdown significantly inhibited cell proliferation ability (**Figure 1C**, **1D**), and colony formation assays showed that silencing brachyury resulted in fewer colonies (**Figure 1E**, **1F**). We next examined the influence of brachyury on HCC cell migration using a Transwell assay. The number of migrating cells was significantly reduced after brachyury silencing in HepG2 and Huh7 cells (**Figure 1G**, **1H**). Therefore, these data indicated that brachyury knockdown negatively regulates cell growth and migration in HepG2 and Huh7 cells.

Silencing of brachyury inhibits HCC cell proliferation in vivo

To determine whether brachyury affects HCC proliferation *in vivo*, we performed tumor formation experiments in nude mice. Nude mice were injected with Huh7 cells stably transfected with sh-brachyury or sh-NC, and the tumor volumes were calculated every 5 days. The sh-brachyury group exhibited smaller subcutaneous tumors than those in the control group (**Figure 2A-C**). Immunofluorescence staining of brachyury showed a significant decrease in its expression in sh-brachyury tumor tissues compared with that in the sh-NC group (Figure S2). To investigate the role of brachyury in promoting cell proliferation *in vivo*, we utilized immunofluorescence staining to measure the Ki-67 protein level. In brachyury-deficient tumor tissues, a significant decrease in the number of Ki-67-positive ($Ki\text{-}67^+$) cells was observed (**Figure 2D**, **2E**), indicating that brachyury knockdown suppresses cell proliferation *in vivo*.

Brachyury directly binds to the NCAPG2 promoter region to positively regulate its expression

Our previous study found that brachyury is an important transcriptional regulator and that it plays an oncogenic role in breast cancer by directly binding to the SOX5 promoter region [10]. To explore whether brachyury has a similar transcriptional regulatory function in HCC cells, we reanalyzed the DNA regions that the brachyury transcriptional factor interacts with that were identified in our previously reported ChIP-seq data [10], and we used qRT-PCR to examine 60 potential target molecules whose expression is regulated by brachyury (**Figure 3A**). We found that, among the 60 potential target molecules, only NCAPG2 levels were significantly reduced when brachyury was silenced in both HepG2 and Huh7 cells (**Figure 3B**). Additionally, we identified a brachyury-binding peak at the promoter region of NCAPG2 (**Figure 3C**). The enrichment of brachyury on the promoter region of NCAPG2 was detected in HepG2 and

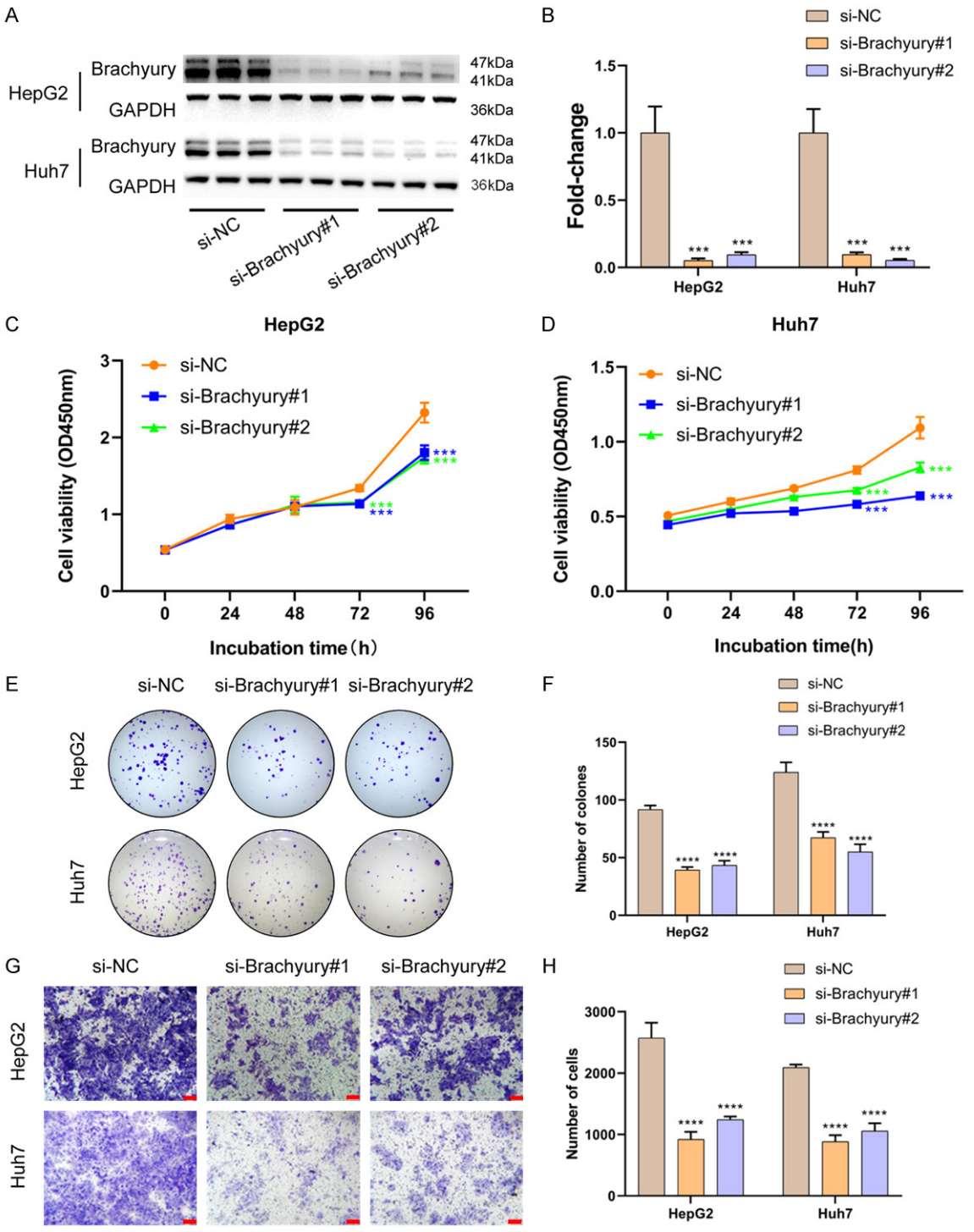

Figure 1. Brachyury knockdown decreases HCC cell proliferation and migration *in vitro*. A, B. Western blot analysis was utilized to confirm the siRNA-mediated knockdown of brachyury in HepG2 and Huh7 cells. C, D. CCK8 assays revealed that brachyury knockdown attenuated the growth of both HepG2 and Huh7 cells for up to 96 h compared to that of the si-NC group. E, F. Colony formation assays were performed to determine the proliferation ability of si-brachyury-transfected HepG2 and Huh7 cells. G, H. Transwell assays were performed to investigate the changes in migration abilities of si-brachyury-transfected HepG2 and Huh7 cells. Scale bar = 100 μm. ***P < 0.001 and ****P < 0.01.

Huh7 cells using a ChIP-qPCR assay (**Figure 3D**, **3E**). Further bioinformatics analysis identified two functional motifs, namely, 5'-BTGG-GARR-3' and 5'-YGCCTGW-3', which are highly

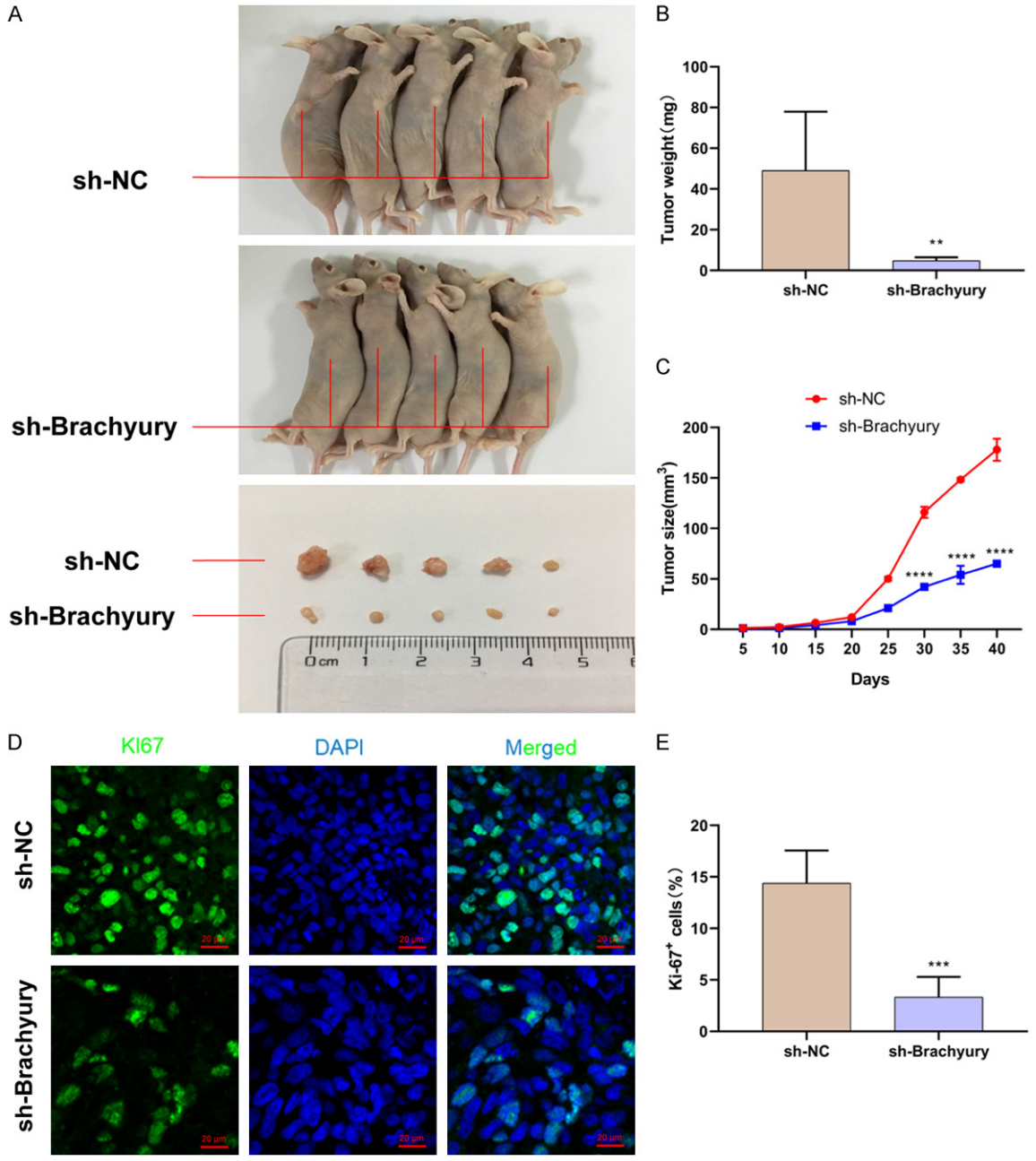

Figure 2. Silencing of brachyury inhibits HCC cell proliferation *in vivo*. Brachyury-deficient or control Huh7 cells were subcutaneously injected into nude mice. A. Tumors were then collected and photographed. B. Tumor weights were measured in the control group and brachyury-deficient group. C. Tumor volumes were calculated every 5 days after injection. D, E. Ki-67 expression in the control and brachyury-deficient groups was evaluated by immunofluorescence and DAPI staining. Scale bar = 20 μm. **P < 0.01, ***P < 0.001, and ****P < 0.0001.

conserved among humans, macaques, mice, and rats, in the binding peak of NCAPG2 (**Figure 3F**). For further confirmation, we generated constructs containing the NCAPG2 promoter sequence that lacked the two motifs (mut-1 and mut-2) and performed a dual-luciferase reporter assay, which showed that the mutated NCAPG2 promoter significantly attenuated the brachyury-mediated transcriptional activation of NCAPG2 (**Figure 3G**). Collectively, these findings demonstrated that brachyury positively regulates NCAPG2 transcription through binding to two specific motifs in its promoter region. Finally, we examined the NCAPG2 levels in brachyury-deficient tumor tissues. Compared with the sh-NC group, the

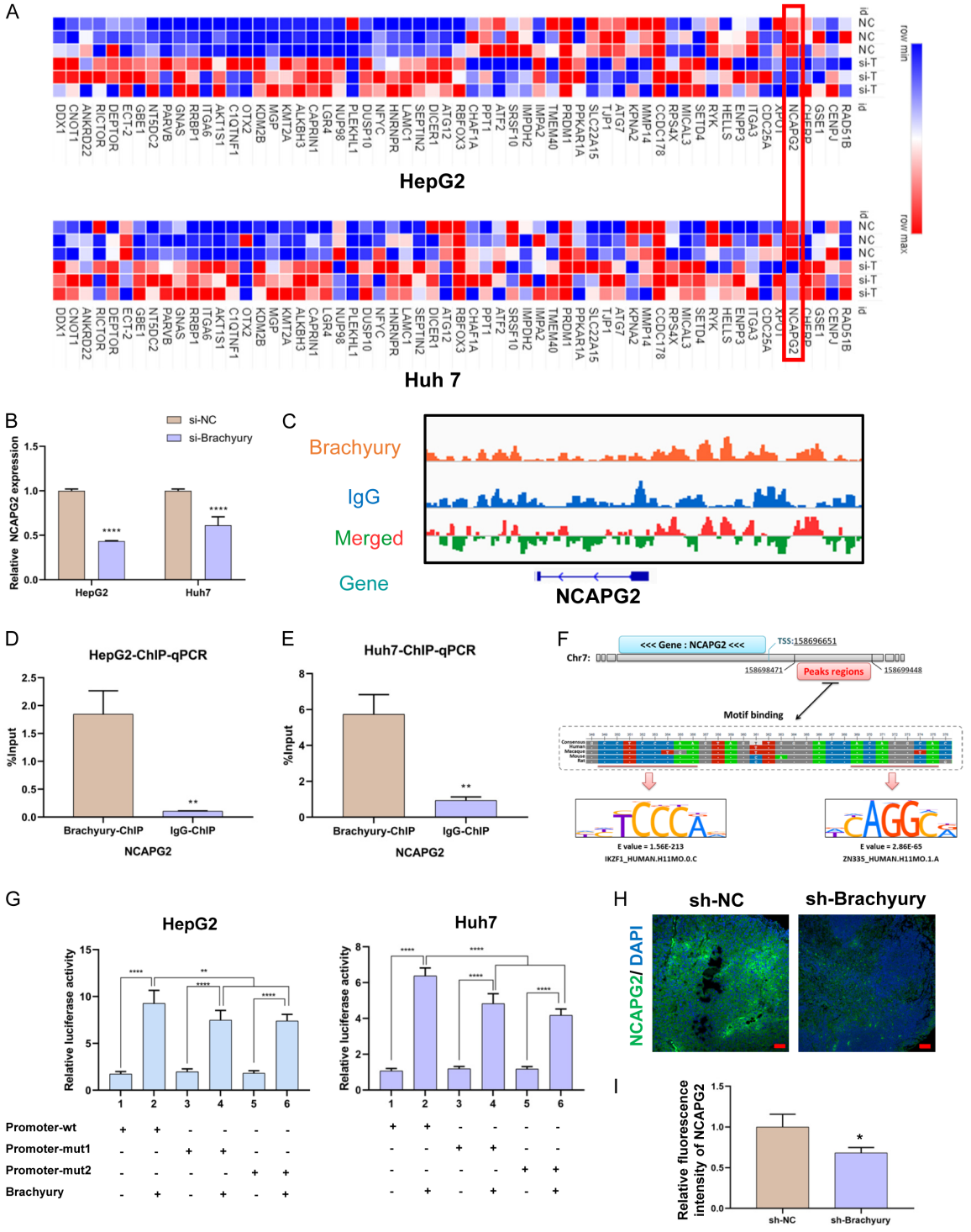

Figure 3. Brachyury positively regulates NCAPG2 transcription via binding to two specific motifs in the NCAPG2 promoter region. (A) Relative expression of candidate genes in the si-NC group compared to the si-brachyury group according to qRT-PCR analysis. (B) Relative expression of NCAPG2 in the si-NC group compared to that in the si-brachyury group according to qRT-PCR analysis. (C) The binding peak of brachyury in the NCAPG2 promoter region. (D, E) ChIP-qPCR analysis of brachyury-associated DNA sequences of the putative brachyury-binding region of the NCAPG2 promoter in HepG2 and Huh7 cells. (F) Sequence analysis of the putative brachyury-binding region. (G) Luciferase activity assays in HepG2 and Huh7 cells transfected with pGL3-NCAPG2 wild-type (wt), mutant (mut), and pcDNA3.0-brachyury plasmids for 48 h. (H) Immunofluorescence staining of NCAPG2 in sh-NC and sh-brachyury tumor tissues. (I) Quantification of (H). Scale bar = 50 μm. *P < 0.05, **P < 0.01 and ****P < 0.0001.

NCAPG2 expression levels were significantly decreased in brachyury-deficient tumor tissues (**Figure 3H**, **3I**).

NCAPG2 knockdown represses cell proliferation and migration of HCC cells

To confirm the regulation of HCC progression by NCAPG2, NCAPG2 siRNAs were transfected into HepG2 and Huh7 cells (**Figure 4A**), which demonstrated that NCAPG2 knockdown decreased HCC cell proliferation (**Figure 4B-E**). Using a Transwell assay, we demonstrated that NCAPG2 silencing significantly suppressed HepG2 and Huh7 cell migration (**Figure 4F**, **4G**). Taken together, these results demonstrated that NCAPG2 plays a major role in promoting HCC progression.

NCAPG2 silencing reverses the effects of brachyury overexpression in HCC cells

To investigate whether brachyury promotes HCC progression via facilitating NCAPG2 transcription, we performed a rescue experiment to observe the changes in HCC cell proliferation and migration. The brachyury overexpression plasmid was cotransfected with si-NCAPG2 into HepG2 and Huh7 cells followed by functional analysis using CCK-8, colony formation, and Transwell assays. The proliferation (**Figure 5A-D**) and migration (**Figure 5E**, **5F**) of HepG2 and Huh7 cells were enhanced by overexpressing brachyury alone, but these effects were suppressed with siNCAPG2 cotransfection.

NCAPG2 is significantly upregulated in HCC patients and affects their prognosis

The above results in HCC cell lines suggested that NCAPG2, as a brachyury target gene, may affect the biological behavior of tumors, including cell proliferation and colony formation, but NCAPG2 expression in HCC patients and its correlation with the clinical stage and prognosis remain unclear. Therefore, we evaluated the expression of NCAPG2 as well as its correlation with prognosis in HCC using three databases, including TCGA, GTEx, and GEO.

Data mining of TCGA and the GTEx database indicated that the NCAPG2 mRNA levels in HCC tissues were significantly greater than those in normal tissues (**Figure 6A**). In addition, analysis of the GSE62232, GSE101685, and GSE112790 GEO datasets demonstrated that NCAPG2 was highly expressed in HCC ($p < 0.001$) (**Figure 6B-D**). Overall, these results indicated that NCAPG2 is overexpressed in HCC compared with normal tissues.

NCAPG2 expression significantly increased with increasing T stage (**Figure 6E**), pTNM stage (**Figure 6F**), and histological grade (**Figure 6G**). Patients with a more advanced HCC stage tended to have high NCAPG2 expression levels, and increased NCAPG2 expression was correlated with HBV infection (**Figure 6H**).

Using the median value of NCAPG2 expression as the cutoff point, patients were divided into high and low expression groups. We then evaluated the relationship between NCAPG2 expression and HCC survival outcomes based on TCGA database. According to the KM survival analysis, HCC patients with high NCAPG2 expression levels (high expression group) had significantly shorter OS [HR = 1.71 (1.20-2.43), log-rank P = 0.003; **Figure 6I**], PFS [HR = 1.73 (1.28-2.32), log-rank P = 3e-04; **Figure 6J**], and DFS [HR = 1.68 (1.21-2.34), log-rank P = 0.002; **Figure 6K**] than those in the low expression group. In addition, **Figure 6I-K** show the survival time and survival status corresponding to NCAPG2 expression in all HCC patients using scatterplots. Thus, these data indicated that overexpression of NCAPG2 is associated with a poor prognosis.

Immune cell infiltration and immune checkpoint molecules are correlated with NCAPG2 expression in HCC patients

Because immune cells are an important part of the tumor microenvironment (TME), we used the TIMER algorithm to explore the relationship of NCAPG2 expression with immune cell infiltration in HCC. The correlation between NCAPG2 expression and immune cell infiltrates was analyzed using Spearman correlation analysis. We found that NCAPG2 expression was positively correlated with infiltrating levels of B cells (r = 0.25, P = 1.52e-06), $CD4^+$ T-cells (r = 0.24, P = 3.37e-06), neutrophils (r = 0.33, P = 1.17e-10), macrophages (r = 0.31, P = 1.35e-09), and dendritic cells (DCs) (r = 0.30, P = 1.43e-04) in HCC but not with $CD8^+$ T-cells (r = 0.10, P = 0.06) (**Figure 7A**). Using the quanTIseq algorithm, we also found that NCAPG2 expression was positively correlated with mac-

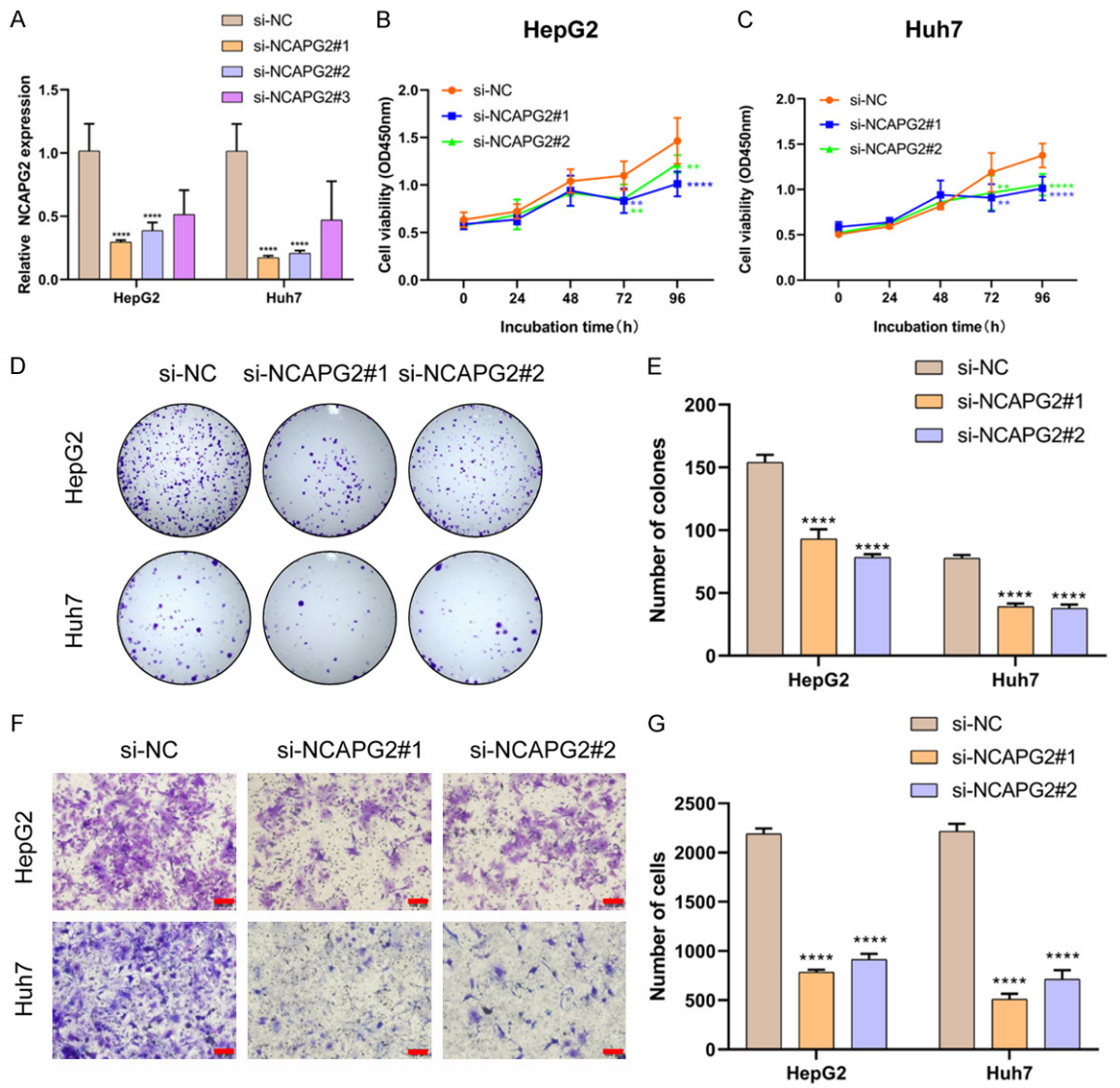

Figure 4. Knockdown of NCAPG2 represses cell proliferation and colony formation in HCC cells. A. NCAPG2 mRNA levels were detected after si-RNA transfection. B, C. CCK8 assays revealed that NCAPG2 knockdown attenuated the growth of both HepG2 and Huh7 cells up to 96 h compared to that of the si-NC group. D, E. Colony formation assays were performed to determine the proliferation ability of si-NCAPG2-transfected HepG2 and Huh7 cells. F, G. Transwell assays were performed to investigate changes in the migration abilities of si-NCAPG2-transfected HepG2 and Huh7 cells. Scale bar = 100 μm. **P < 0.01 and ****P < 0.0001.

rophage M2 polarization (**Figure 7B**). Further analysis showed that NCAPG2 expression was correlated with M2-like macrophage markers, including CD163 and TGFB1 (**Figure 7C**, **7D**). As a major component of the TME, CAFs are closely related to tumor prognosis and the immune response [33]. Therefore, we explored the correlation between NCAPG2 expression and CAFs in HCC using the TIMER 2.0 website (**Figure 7E**), which showed that NCAPG2 expression was positively correlated with CAFs.

The above results suggested that NCAPG2 expression may affect immune therapy. Six immune subtypes based on TCGA immunogenomic analysis can be used to characterize heterogeneous tumors, which may benefit immune therapy and have prognostic implications for cancer management [29]. We found that NCAPG2 expression was associated with the six immune subtypes (**Figure 7F**). In addition, the expression of immune checkpoint molecules on immune cells inhibits their func-

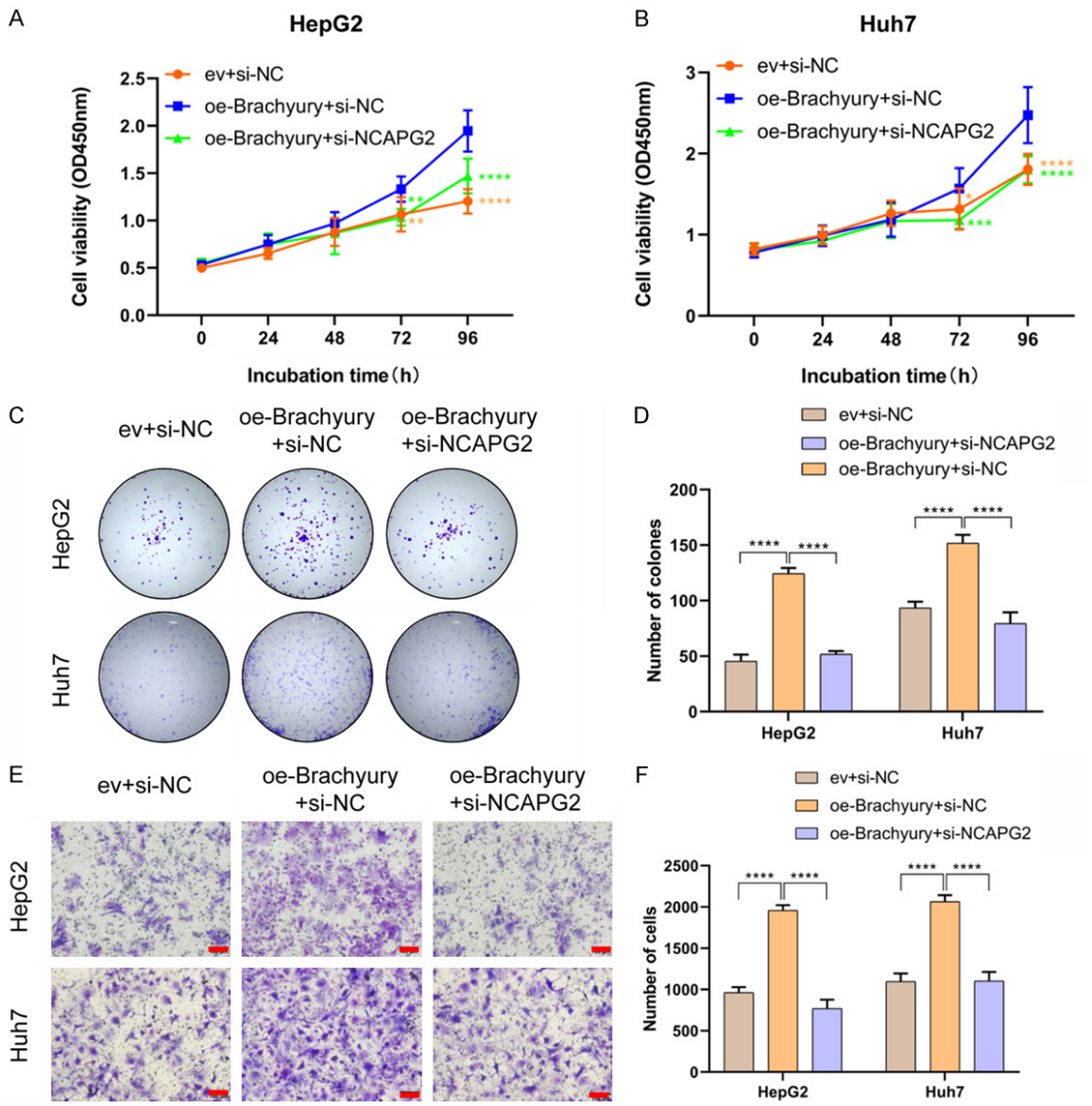

Figure 5. NCAPG2 silencing reverses the effects of brachyury overexpression on HCC cells. Empty vector (ev) plasmid, brachyury overexpression (oe) plasmid, si-NC, and si-NCAPG2 were cotransfected into HCC cells. A, B. CCK8 assays revealed that brachyury overexpression increased the growth of both HepG2 and Huh7 cells up to 96 h compared to that in the control group. Cotransfection of the brachyury-oe plasmid and si-NCAPG2 suppressed the alteration of cell viability. C, D. Colony formation assays were performed to determine the proliferation ability of HepG2 and Huh7 cells after cotransfection of the brachyury-oe plasmid and si-NCAPG2. E, F. Transwell assays were performed to investigate changes in the migration abilities of HepG2 and Huh7 cells after cotransfection of the brachyury-oe plasmid and si-NCAPG2. Scale bar = 100 μm. *P < 0.05, **P < 0.01, ***P < 0.001, and ****P < 0.0001.

tion and mediates tumor immune escape. In the present study, the expression levels of immune checkpoint molecules, including CD274, CTLA4, HAVCR2, LAG3, PDCD1, PDCD1LG2, TIGIT, and SIGLEC15, were upregulated in tumor tissues with high NCAPG2 expression compared with those in tumor tissues with low NCAPG2 expression (**Figure 7G**), suggesting that NCAPG2 is positively correlated with immune checkpoint molecules and promotes immune escape of HCC tumor cells. We also predicted the responsiveness of NCAPG2 gene expression to ICIs using the TIDE algorithm [34]. The TIDE score was higher in the high

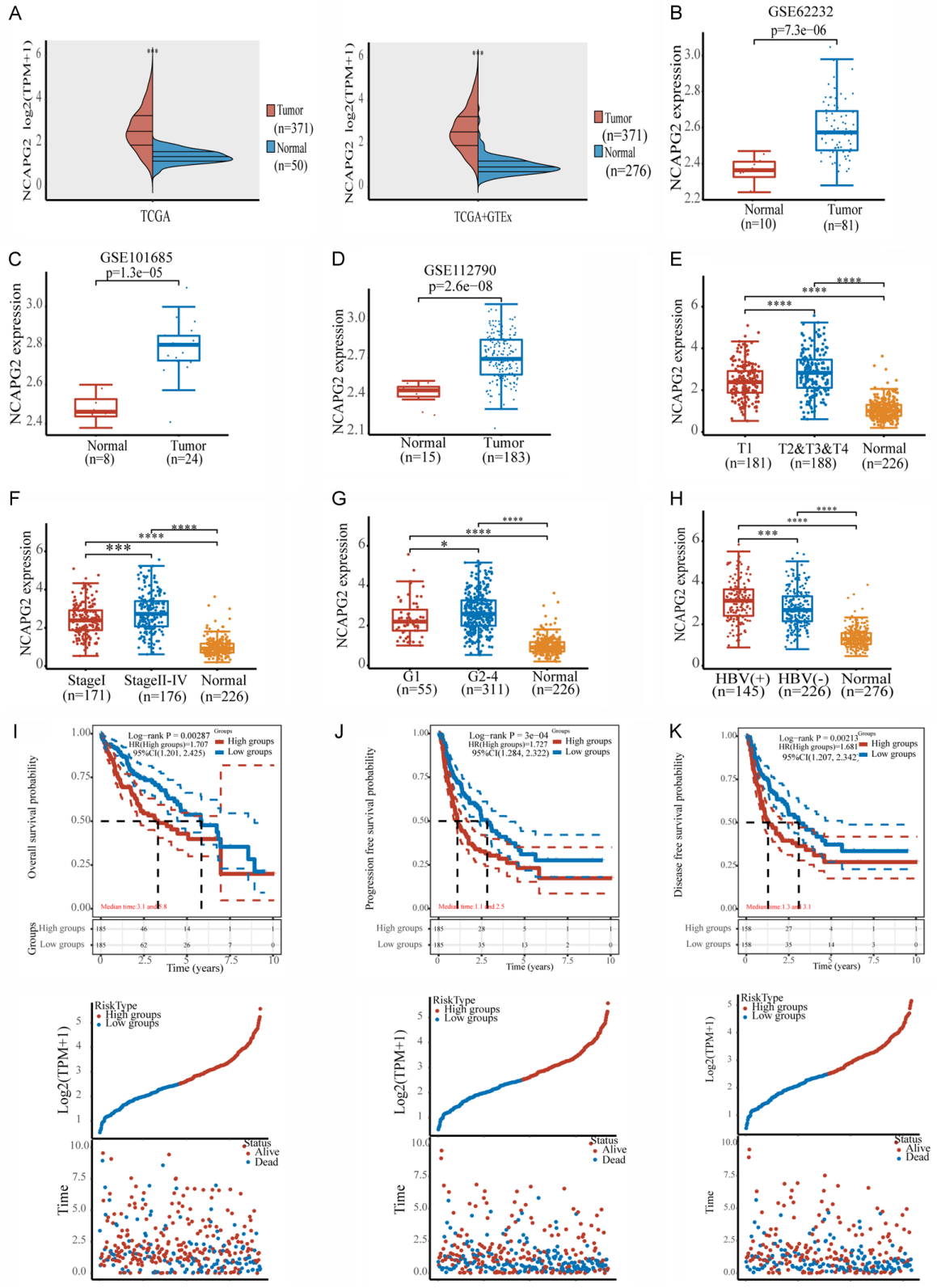

Figure 6. NCAPG2 is significantly upregulated in HCC patients and affects their prognosis. (A) NCAPG2 expression in tumor and normal tissues in TCGA and GTEx data. (B-D) NCAPG2 mRNA levels in the GSE62232, GSE101685, and GSE112790 datasets from the GEO database. (E-H) NCAPG2 expression was correlated with T stage (E), pathological stage (F), histological grade (G), and HBV infection (H). (I-K) According to the KM survival analysis, HCC patients with high NCAPG2 expression (high group) had significantly shorter OS (I), PFS (J), and DFS (K) than those in the low NCAPG2 expression group. *P < 0.05, **P < 0.01, ***P < 0.001, and ****P < 0.0001.

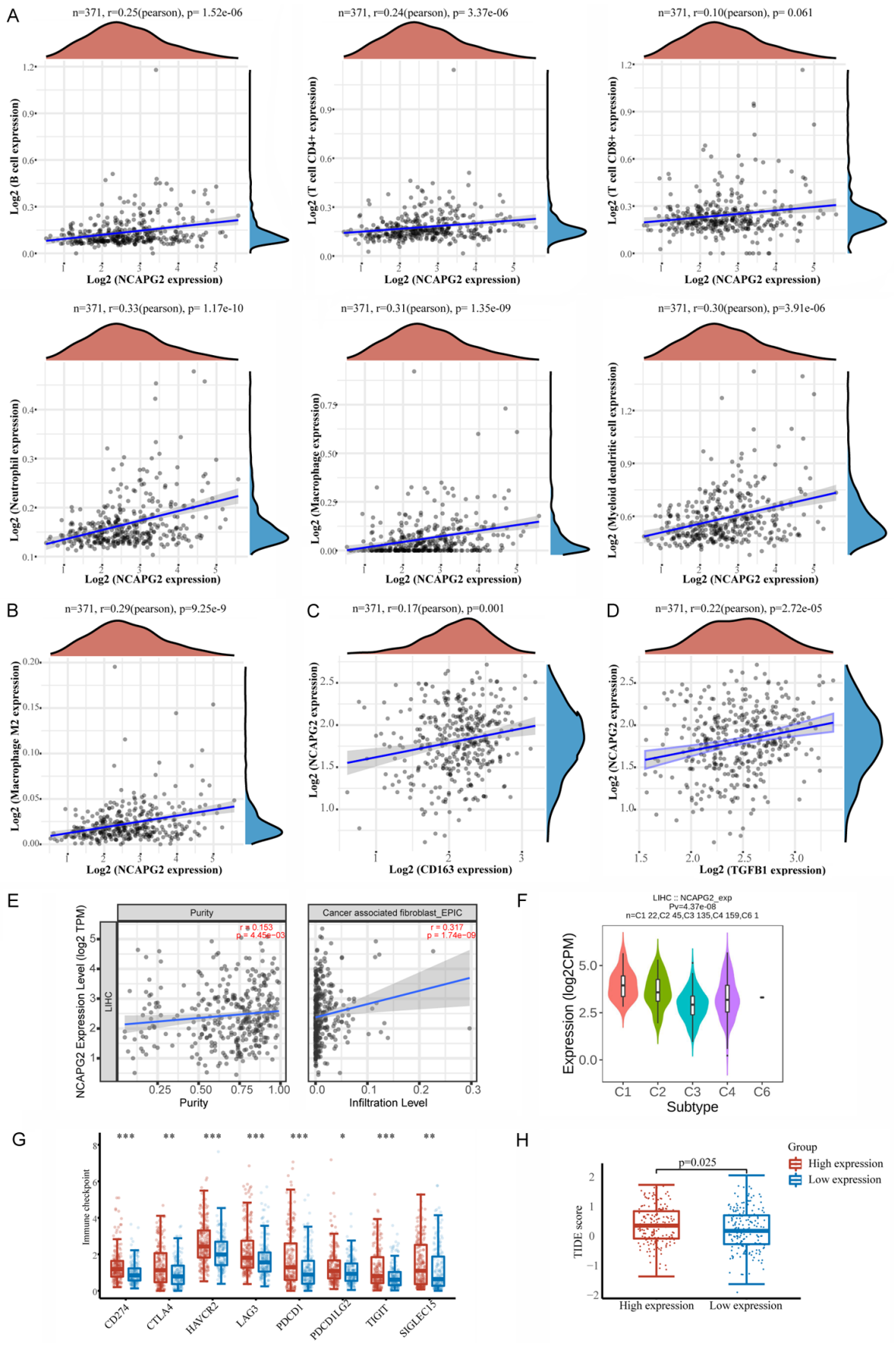
A
n=371, r=0.25(pearson), p= 1.52e-06
Log2 (B cell expression)
Log2 (NCAPG2 expression)
n=371, r=0.24(pearson), p= 3.37e-06
Log2 (T cell CD4+ expression)
Log2 (NCAPG2 expression)
n=371, r=0.10(pearson), p= 0.061
Log2 (T cell CD8+ expression)
Log2 (NCAPG2 expression)
n=371, r=0.33(pearson), p= 1.17e-10
Log2 (Neutrophil expression)
Log2 (NCAPG2 expression)
n=371, r=0.31(pearson), p= 1.35e-09
Log2 (Macrophage expression)
Log2 (NCAPG2 expression)
n=371, r=0.30(pearson), p=3.91e-06
Log2 (Myeloid dendritic cell expression)
Log2 (NCAPG2 expression)
B
n=371, r=0.29(pearson), p=9.25e-9
Log2 (Macrophage M2 expression)
Log2 (NCAPG2 expression)
C
n=371, r=0.17(pearson), p=0.001
Log2 (NCAPG2 expression)
Log2 (CD163 expression)
D
n=371, r=0.22(pearson), p=2.72e-05
Log2 (NCAPG2 expression)
Log2 (TGFB1 expression)
E
Purity
r = 0.153
p = 4.45e-03
Cancer associated fibroblast_EPIC
r = 0.317
p = 1.74e-09
NCAPG2 Expression Level (log2 TPM)
LIHC
Purity
Infiltration Level
F
LIHC :: NCAPG2_exp
P=4.37e-08
n=C1 22,C2 45,C3 135,C4 159,C6 1
Expression (log2CPM)
C1
C2
C3
C4
C6
Subtype
G
Immune checkpoint
CD274
CTLA4
HAVCR2
LAG3
PDCD1
PDCD1LG2
TIGIT
SIGLEC15
H
p=0.025
Group
High expression
Low expression
TIDE score
High expression
Low expression

Figure 7. Immune cell infiltration and immune checkpoint molecules are correlated with NCAPG2 expression in HCC patients. (A) Correlation between immune cell infiltration and NCAPG2 expression in HCC patients. (B) Correlation between NCAPG2 expression and macrophage M2 polarization according to quanTIseq algorithms. (C, D) Correlation between NCAPG2 expression and M2-like macrophage markers, including CD163 (C) and TGFB1 (D). (E) Correlation between NCAPG2 expression and CAFs according to the TIMER 2.0 website. (F) NCAPG2 expression in different molecular subtypes, including wound healing (C1), IFN-gamma dominant (C2), inflammatory (C3), lymphocyte depleted (C4), immunologically quiet (C5), and TGF-beta dominant (C6). (G) Correlation between NCAPG2 expression and immune checkpoint molecules, including CD274, CTLA4, HAVCR2, LAG3, PDCD1, PDCD1LG2, TIGIT, and SIGLEC15. (H) Responsiveness of NCAPG2 expression to ICIs according to the TIDE algorithm. *P < 0.05, **P < 0.01, and ***P < 0.001.

NCAPG2 expression group than that in the low NCAPG2 expression group (**Figure 7H**), suggesting that immune checkpoint blockade (ICB) is less effective in the high NCAPG2 expression group.

NCAPG2 methylation, the stemness index, and pathway enrichment analysis results are correlated with NCAPG2 expression in HCC patients

DNA methylation is a common epigenetic mechanism affecting tumorigenesis and development. Therefore, we investigated the relationship between DNA methylation levels of NCAPG2 and the prognosis of patients using the MethSurv tool. A high methylation level of two CpG sites, namely, cg11951909 and cg05703659, was correlated with significantly longer OS (P < 0.05) (**Figure 8A**).

Because tumor stemness is thought to be responsible for tumor growth, maintenance, metastasis, and recurrence, we assessed the tumor stemness score using the OCLR algorithm and analyzed the correlation between NCAPG2 expression and stemness scores in HCC patients. Compared to normal tissues, the tumor stemness score was significantly increased in both the high and low NCAPG2 expression groups, and NCAPG2 overexpression resulted in a significantly increased tumor stemness score (**Figure 8B**).

To elucidate the potential signaling pathways including NCAPG2, we evaluated the correlation between NCAPG2 and pathway scores in HCC patients in TCGA using GSEA. NCAPG2 expression was positively correlated with the tumor proliferation signature, DNA repair, G2M checkpoint, PI3K-AKT-mTOR pathway, MYC target, and DNA replication scores (**Figure 8C**), suggesting that the mechanisms of NCAPG2 that affect HCC progression occur through these signaling pathways.

Discussion

Effect of brachyury on the oncogenic properties of HCC

Brachyury, which was the first identified T-box family member, is aberrantly expressed in various solid tumors and is associated with tumor aggressiveness and a poor prognosis [35]. In particular, brachyury mRNA has previously been shown to be overexpressed in lung cancer tissues and correlated with a poor prognosis for both 5-year DFS and OS in primary lung carcinoma patients [12, 36]. Brachyury also promotes lung cancer tumor cell proliferation and invasion but inhibits lung cancer cell apoptosis [37, 38]. In addition, brachyury is overexpressed in prostate [39], colorectal [40], and oral cancer [41]. Interestingly, brachyury was reported to be significantly downregulated in glioma tissues [42]. Loss of brachyury is correlated with tumor aggressiveness and poor survival in glioma patients [42].

Brachyury expression is upregulated in HCC [16], and high brachyury expression levels are correlated with tumor size, intrahepatic invasion, and distance metastasis [16]. Moreover, brachyury overexpression contributes to tumor metastasis by inducing EMT in HCC [16]. In the present study, we showed that brachyury knockdown inhibited cell proliferation *in vitro* and *in vivo*. We also explored the function of brachyury during HCC migration by examining the migration ability of HepG2 and Huh7 cells using a Transwell assay. Brachyury-deficient cells had slower migration rates, suggesting that brachyury plays a role in HCC metastasis and is a tumor promotor of HCC.

Brachyury directly binds to the NCAPG2 promoter region and affects the malignancy of HCC

To explore the potential mechanism of brachyury, we reanalyzed the DNA regions that bra-

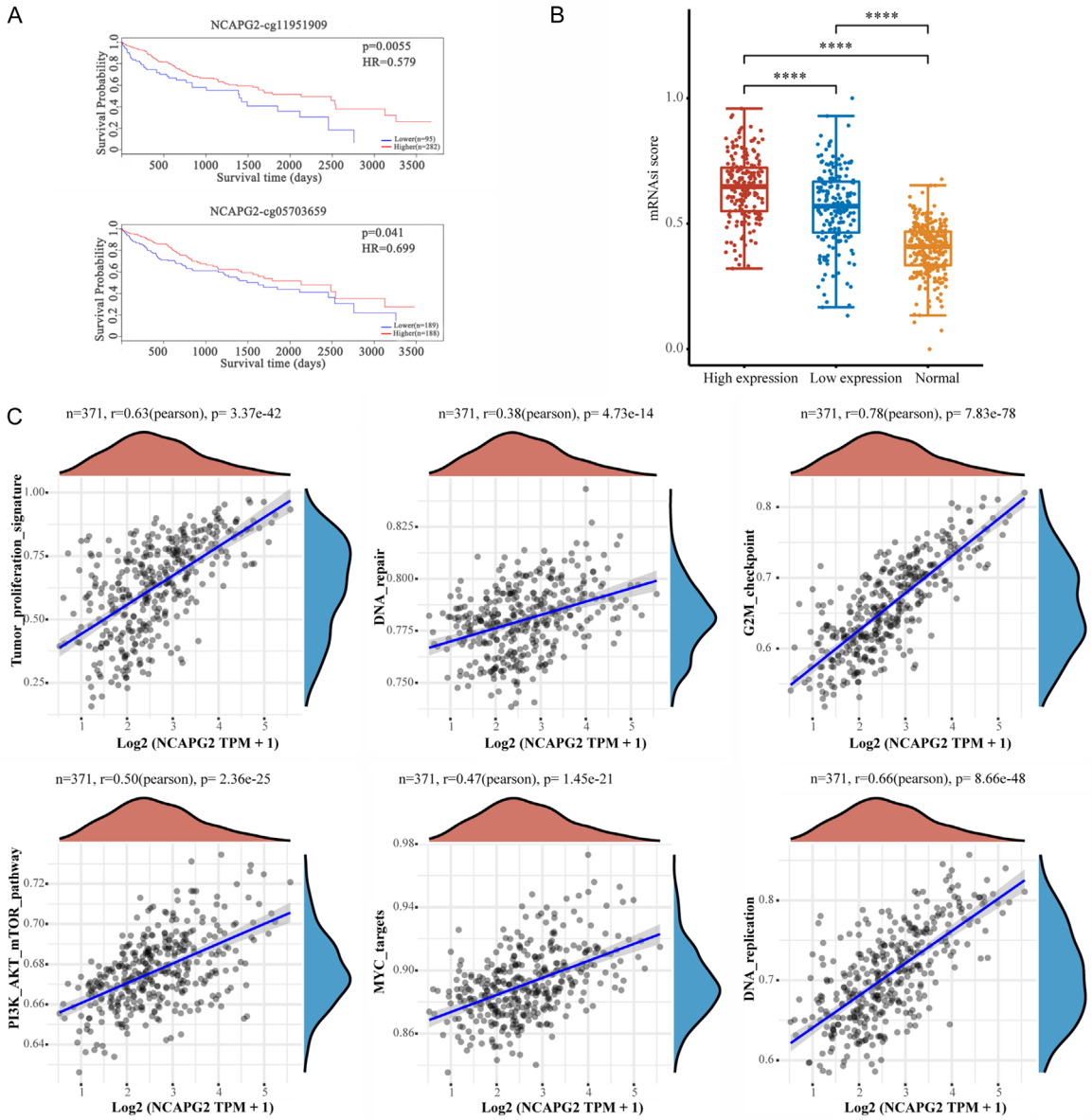

Figure 8. NCAPG2 methylation, the stemness index, and pathway enrichment analysis results are correlated with NCAPG2 expression. A. A high methylation level of two CpG sites, cg11951909 and cg05703659, resulted in significantly longer OS. B. Correlation between NCAPG2 expression and stemness scores. C. Correlation between NCAPG2 expression and pathway scores in HCC patients in TCGA according to GSEA. ****P < 0.0001.

chyury interacts with that were identified in our previously published ChIP-seq data [10], and we performed qRT-PCR assays to examine 60 potential target molecules whose expression is regulated by brachyury. Notably, we found that brachyury silencing led to a significant decrease in the NCAPG2 level. Moreover, we found that brachyury has two binding regions, 5'-BTGGGARR-3' and 5'-YGCCTGW-3, within the NCAPG2 promoter. We generated constructs containing the NCAPG2 promoter sequence that lacked these two motifs and used a dual-luciferase reporter assay to show that the mutated NCAPG2 promoter significantly attenuated brachyury-mediated transcriptional activation of NCAPG2, suggesting that NCAPG2 is a direct downstream target of brachyury.

NCAPG2 is part of the chromosome condensin II complex, which is critical for chromosome condensation and segregation during mitosis [18]. Recent studies have found that NCAPG2

is upregulated in several tumors and is associated with malignant behaviors of cancer [17, 40, 43]. In particular, Meng et al. reported that NCAPG2 overexpression drives HCC proliferation and metastasis through activation of the STAT3 and NF-κB/miR-188-3p pathways [18]. In addition, miR-375 is significantly downregulated but NCAPG2 is upregulated in HCC tissues and cells compared to that in adjacent tissues and normal hepatocyte cell lines, respectively. Rescue with miR-375 overexpression significantly repressed HCC cell proliferation and migration and induced cell apoptosis, and NCAPG2 overexpression rescued the biological abilities in cells with miR-375 overexpression, suggesting that miR-375 serves as a tumor suppressor via regulating NCAPG2 [19]. In the present study, we found that NCAPG2 silencing repressed cell proliferation and colony formation, inhibited proliferation and migration of HCC cells, and attenuated brachyury-induced tumorigenesis. Based on clinical samples from TCGA and the GEO databases, we verified that NCAPG2 is overexpressed in HCC tissues. Moreover, an elevated expression level of NCAPG2 was significantly correlated with cancer stage and HBV infection. NCAPG2 overexpression and decreased DNA methylation of NCAPG2 were associated with a poor prognosis. In addition, NCAPG2 was positively correlated with tumor stemness. Pathway enrichment analysis indicated that NCAPG2 expression was positively correlated with the tumor proliferation signature, DNA repair, G2M checkpoint, PI3K-AKT-mTOR pathway, MYC target, and DNA replication scores, suggesting that these pathways are closely related to HCC progression. Taken together, these results suggested that brachyury directly binds to the NCAPG2 promoter region and affects the malignancy of HCC.

NCAPG2 influences HCC progression by affecting the TME

The TME, which specifically refers to the local environment where tumors occur and develop [44], is composed of immune components, vascular components, stromal cells, and the extracellular matrix [44]. The TME plays various roles in HCC development, progression, and recurrence after multiple therapies [45]. To determine the function of NCAPG2 in HCC, we explored the correlations of immune cell infiltration, CAFs, and immune checkpoint molecules with NCAPG2 expression. NCAPG2 was positively correlated with various immune cell infiltrates, such as B cells, $CD4^+$ T-cells, neutrophils, macrophages, and DCs. In particular, NCAPG2 expression was positively correlated with macrophage M2 polarization and M2-like macrophage marker genes. We also explored the correlation between NCAPG2 expression and CAFs, as a major component of the TME, and demonstrated that NCAPG2 expression was positively correlated with CAFs.

The expression of immune checkpoint molecules on immune cells inhibits the function of these cells and mediates tumor immune escape. In addition, ICIs have demonstrated significant survival benefits in HCC patients. As expected, the expression levels of immune checkpoint molecules, including CD274, CTLA4, HAVCR2, LAG3, PDCD1, PDCD1LG2, TIGIT, and SIGLEC15, were upregulated in tumor tissues with high NCAPG2 expression. Moreover, we also predicted the responsiveness of NCAPG2 gene expression to ICIs using the TIDE algorithm and demonstrated that ICB was less effective in the high NCAPG2 expression group.

Conclusions

The present study showed that brachyury promotes NCAPG2-mediated proliferation and migration during HCC progression. We also found that NCAPG2 overexpression and reduced DNA methylation of NCAPG2 were associated with a poor prognosis. NCAPG2 was positively correlated with various immune cell infiltrates, CAFs, and immune checkpoint molecule expression levels in the TME. Moreover, ICB was less effective in the high NCAPG2 expression group. These findings provide a potential novel target for the diagnosis and treatment of HCC.

Acknowledgements

This study was funded by the National Natural Science Foundation of China (81901533) and the Suzhou Clinical Medical Center Construction Project (SZLCYXZXJ202107).

Disclosure of conflict of interest

None.

Address correspondence to: Drs. Xinwei Jiang and Jianwu Wu, Department of Hepatobiliary Surgery, Suzhou Municipal Hospital, The Affiliated Suzhou Hospital of Nanjing Medical University, Gusu School, Nanjing Medical University, Suzhou 215002, China. Tel: +86-051262362004; E-mail: jxw19681022@163.com (XWJ); wusi1981@njmu.edu.cn (JWW)

References

[1] Sung H, Ferlay J, Siegel RL, Laversanne M, Soerjomataram I, Jemal A and Bray F. Global cancer statistics 2020: GLOBOCAN estimates of incidence and mortality worldwide for 36 cancers in 185 countries. CA Cancer J Clin 2021; 71: 209-249.

[2] Nakano M, Yatsuhashi H, Bekki S, Takami Y, Tanaka Y, Yoshimaru Y, Honda K, Komorizono Y, Harada M, Shibata M, Sakisaka S, Shakado S, Nagata K, Yoshizumi T, Itoh S, Sohda T, Oeda S, Nakao K, Sasaki R, Yamashita T, Ido A, Mawatari S, Nakamuta M, Aratake Y, Matsumoto S, Maeshiro T, Goto T and Torimura T. Trends in hepatocellular carcinoma incident cases in Japan between 1996 and 2019. Sci Rep 2022; 12: 1517.

[3] Zuo Z, Chen T, Zhang Y, Han L, Liu B, Yang B, Han T and Zheng Z. Construction of a ceRNA network in hepatocellular carcinoma and comprehensive analysis of immune infiltration patterns. Am J Transl Res 2021; 13: 13356-13379.

[4] Liu TH, Shao YY and Hsu CH. It takes two to tango: breakthrough advanced hepatocellular carcinoma treatment that combines anti-angiogenesis and immune checkpoint blockade. J Formos Med Assoc 2021; 120: 1-4.

[5] Zhang T, Zhang L, Xu Y, Lu X, Zhao H, Yang H and Sang X. Neoadjuvant therapy and immunotherapy strategies for hepatocellular carcinoma. Am J Cancer Res 2020; 10: 1658-1667.

[6] Showell C, Binder O and Conlon FL. T-box genes in early embryogenesis. Dev Dyn 2004; 229: 201-218.

[7] Papaioannou VE. The T-box gene family: emerging roles in development, stem cells and cancer. Development 2014; 141: 3819-3833.

[8] Vujovic S, Henderson S, Presneau N, Odell E, Jacques TS, Tirabosco R, Boshoff C and Flanagan AM. Brachyury, a crucial regulator of notochordal development, is a novel biomarker for chordomas. J Pathol 2006; 209: 157-165.

[9] Romeo S and Hogendoorn PC. Brachyury and chordoma: the chondroid-chordoid dilemma resolved? J Pathol 2006; 209: 143-146.

[10] Chen M, Zou S, He C, Zhou J, Li S, Shen M, Cheng R, Wang D, Zou T, Yan X, Huang Y and Shen J. Transactivation of SOX5 by brachyury promotes breast cancer bone metastasis. Carcinogenesis 2020; 41: 551-560.

[11] Li K, Ying M, Feng D, Du J, Chen S, Dan B, Wang C and Wang Y. Brachyury promotes tamoxifen resistance in breast cancer by targeting SIRT1. Biomed Pharmacother 2016; 84: 28-33.

[12] Roselli M, Fernando RI, Guadagni F, Spila A, Alessandroni J, Palmirotta R, Costarelli L, Litzinger M, Hamilton D, Huang B, Tucker J, Tsang KY, Schlom J and Palena C. Brachyury, a driver of the epithelial-mesenchymal transition, is overexpressed in human lung tumors: an opportunity for novel interventions against lung cancer. Clin Cancer Res 2012; 18: 3868-3879.

[13] Pinto F, Pértega-Gomes N, Pereira MS, Vizcaíno JR, Monteiro P, Henrique RM, Baltazar F, Andrade RP and Reis RM. T-box transcription factor brachyury is associated with prostate cancer progression and aggressiveness. Clin Cancer Res 2014; 20: 4949-4961.

[14] Pinto F, Cárcano FM, da Silva ECA, Vidal DO, Scapulatempo-Neto C, Lopes LF and Reis RM. Brachyury oncogene is a prognostic factor in high-risk testicular germ cell tumors. Andrology 2018; 6: 597-604.

[15] Sarkar D, Shields B, Davies ML, Müller J and Wakeman JA. BRACHYURY confers cancer stem cell characteristics on colorectal cancer cells. Int J Cancer 2012; 130: 328-337.

[16] Du R, Wu S, Lv X, Fang H, Wu S and Kang J. Overexpression of brachyury contributes to tumor metastasis by inducing epithelial-mesenchymal transition in hepatocellular carcinoma. J Exp Clin Cancer Res 2014; 33: 105.

[17] Kim JH, Shim J, Ji MJ, Jung Y, Bong SM, Jang YJ, Yoon EK, Lee SJ, Kim KG, Kim YH, Lee C, Lee BI and Kim KT. The condensin component NCAPG2 regulates microtubule-kinetochore attachment through recruitment of polo-like kinase 1 to kinetochores. Nat Commun 2014; 5: 4588.

[18] Meng F, Zhang S, Song R, Liu Y, Wang J, Liang Y, Wang J, Han J, Song X, Lu Z, Yang G, Pan S, Li X, Liu Y, Zhou F, Wang Y, Cui Y, Zhang B, Ma K, Zhang C, Sun Y, Xin M and Liu L. NCAPG2 overexpression promotes hepatocellular carcinoma proliferation and metastasis through activating the STAT3 and NF-κB/miR-188-3p pathways. EBioMedicine 2019; 44: 237-249.

[19] Dai HT, Wang ST, Chen B, Tang KY, Li N, Wen CY, Wan Y, Zhang GY, Huang YH and Geng ZJ. microRNA-375 inhibits the malignant behaviors of hepatic carcinoma cells by targeting NCAPG2. Neoplasma 2022; 69: 16-27.

[20] Zhao D, Shen C, Gao T, Li H, Guo Y, Li F, Liu C, Liu Y, Chen X, Zhang X, Wu Y, Yu Y, Lin M, Yuan Y, Huang X, Yang S, Yu J, Zhang J and Zheng B. Myotubularin related protein 7 is essential for

the spermatogonial stem cell homeostasis via PI3K/AKT signaling. Cell Cycle 2019; 18: 2800-2813.
[21] Gao T, Lin M, Shao B, Zhou Q, Wang Y, Chen X, Zhao D, Dai X, Shen C, Cheng H, Yang S, Li H, Zheng B, Zhong X, Yu J, Chen L and Huang X. BMI1 promotes steroidogenesis through maintaining redox homeostasis in mouse MLTC-1 and primary leydig cells. Cell Cycle 2020; 19: 1884-1898.
[22] Wang Q, Wu Y, Lin M, Wang G, Liu J, Xie M, Zheng B, Shen C and Shen J. BMI1 promotes osteosarcoma proliferation and metastasis by repressing the transcription of SIK1. Cancer Cell Int 2022; 22: 136.
[23] Zhang K, Xu J, Ding Y, Shen C, Lin M, Dai X, Zhou H, Huang X, Xue B and Zheng B. BMI1 promotes spermatogonia proliferation through epigenetic repression of Ptprm. Biochem Biophys Res Commun 2021; 583: 169-177.
[24] Zhou J, Li J, Qian C, Qiu F, Shen Q, Tong R, Yang Q, Xu J, Zheng B, Lv J and Hou J. LINC00624/TEX10/NF-kappaB axis promotes proliferation and migration of human prostate cancer cells. Biochem Biophys Res Commun 2022; 601: 1-8.
[25] Shen C, Yu J, Zhang X, Liu CC, Guo YS, Zhu JW, Zhang K, Yu Y, Gao TT, Yang SM, Li H, Zheng B and Huang XY. Strawberry notch 1 (SBNO1) promotes proliferation of spermatogonial stem cells via the noncanonical Wnt pathway in mice. Asian J Androl 2019; 21: 345-350.
[26] Shen C, Zhang K, Yu J, Guo Y, Gao T, Liu Y, Zhang X, Chen X, Yu Y, Cheng H, Zheng A, Li H, Huang X, Ding X and Zheng B. Stromal interaction molecule 1 is required for neonatal testicular development in mice. Biochem Biophys Res Commun 2018; 504: 909-915.
[27] Yu J, Wu Y, Li H, Zhou H, Shen C, Gao T, Lin M, Dai X, Ou J, Liu M, Huang X, Zheng B and Sun F. BMI1 drives steroidogenesis through epigenetically repressing the p38 MAPK pathway. Front Cell Dev Biol 2021; 9: 665089.
[28] Acharjee A, Agarwal P, Nash K, Bano S, Rahman T and Gkoutos GV. Immune infiltration and prognostic and diagnostic use of LGALS4 in colon adenocarcinoma and bladder urothelial carcinoma. Am J Transl Res 2021; 13: 11353-11363.
[29] Thorsson V, Gibbs DL, Brown SD, Wolf D, Bortone DS, Ou Yang TH, Porta-Pardo E, Gao GF, Plaisier CL, Eddy JA, Ziv E, Culhane AC, Paull EO, Sivakumar IKA, Gentles AJ, Malhotra R, Farshidfar F, Colaprico A, Parker JS, Mose LE, Vo NS, Liu J, Liu Y, Rader J, Dhankani V, Reynolds SM, Bowlby R, Califano A, Cherniack AD, Anastassiou D, Bedognetti D, Mokrab Y, Newman AM, Rao A, Chen K, Krasnitz A, Hu H, Malta TM, Noushmehr H, Pedamallu CS, Bullman S, Ojesina AI, Lamb A, Zhou W, Shen H, Choueiri TK, Weinstein JN, Guinney J, Saltz J, Holt RA, Rabkin CS; Cancer Genome Atlas Research Network, Lazar AJ, Serody JS, Demicco EG, Disis ML, Vincent BG and Shmulevich I. The immune landscape of cancer. Immunity 2018; 48: 812-830, e814.
[30] Kong D, Liu C, Miao X, Wang Y, Ding X and Gong W. Current statuses of molecular targeted and immune checkpoint therapies in hepatocellular carcinoma. Am J Cancer Res 2020; 10: 1522-1533.
[31] Darwiche N. Epigenetic mechanisms and the hallmarks of cancer: an intimate affair. Am J Cancer Res 2020; 10: 1954-1978.
[32] Malta TM, Sokolov A, Gentles AJ, Burzykowski T, Poisson L, Weinstein JN, Kamińska B, Huelsken J, Omberg L, Gevaert O, Colaprico A, Czerwińska P, Mazurek S, Mishra L, Heyn H, Krasnitz A, Godwin AK, Lazar AJ; Cancer Genome Atlas Research Network, Stuart JM, Hoadley KA, Laird PW, Noushmehr H and Wiznerowicz M. Machine learning identifies stemness features associated with oncogenic dedifferentiation. Cell 2018; 173: 338-354, e315.
[33] De P, Aske JC, Dale A, Rojas Espaillat L, Starks D and Dey N. Addressing activation of WNT beta-catenin pathway in diverse landscape of endometrial carcinogenesis. Am J Transl Res 2021; 13: 12168-12180.
[34] Jiang P, Gu S, Pan D, Fu J, Sahu A, Hu X, Li Z, Traugh N, Bu X, Li B, Liu J, Freeman GJ, Brown MA, Wucherpfennig KW and Liu XS. Signatures of T cell dysfunction and exclusion predict cancer immunotherapy response. Nat Med 2018; 24: 1550-1558.
[35] Chen M, Wu Y, Zhang H, Li S, Zhou J and Shen J. The roles of embryonic transcription factor BRACHYURY in tumorigenesis and progression. Front Oncol 2020; 10: 961.
[36] Fernando RI, Litzinger M, Trono P, Hamilton DH, Schlom J and Palena C. The T-box transcription factor Brachyury promotes epithelial-mesenchymal transition in human tumor cells. J Clin Invest 2010; 120: 533-544.
[37] Xu J, Chen M, Wu Y, Zhang H, Zhou J, Wang D, Zou T and Shen J. The role of transcriptional factor brachyury on cell cycle regulation in non-small cell lung cancer. Front Oncol 2020; 10: 1078.
[38] Chen S, Jiao J, Jiang D, Wan Z, Li L, Li K, Xu L, Zhou Z, Xu W and Xiao J. T-box transcription factor Brachyury in lung cancer cells inhibits macrophage infiltration by suppressing CCL2 and CCL4 chemokines. Tumour Biol 2015; 36: 5881-5890.
[39] Nouri M, Ratther E, Stylianou N, Nelson CC, Hollier BG and Williams ED. Androgen-targeted

therapy-induced epithelial mesenchymal plasticity and neuroendocrine transdifferentiation in prostate cancer: an opportunity for intervention. Front Oncol 2014; 4: 370.
[40] Zhan P, Xi GM, Zhang B, Wu Y, Liu HB, Liu YF, Xu WJ, Zhu Q, Cai F, Zhou ZJ, Miu YY, Wang XX, Jin JJ, Li Q, Lv TF and Song Y. NCAPG2 promotes tumour proliferation by regulating G2/M phase and associates with poor prognosis in lung adenocarcinoma. J Cell Mol Med 2017; 21: 665-676.
[41] Yoshihama R, Yamaguchi K, Imajyo I, Mine M, Hiyake N, Akimoto N, Kobayashi Y, Chigita S, Kumamaru W, Kiyoshima T, Mori Y and Sugiura T. Expression levels of SOX2, KLF4 and brachyury transcription factors are associated with metastasis and poor prognosis in oral squamous cell carcinoma. Oncol Lett 2016; 11: 1435-1446.
[42] Pinto F, Costa ÂM, Santos GC, Matsushita MM, Costa S, Silva VA, Miranda-Gonçalves V, Lopes CM, Clara CA, Becker AP, Neder L, Hajj GN, da Cunha IW, Jones C, Andrade RP and Reis RM. The T-box transcription factor brachyury behaves as a tumor suppressor in gliomas. J Pathol 2020; 251: 87-99.
[43] Wu J, Li L, Jiang G, Zhan H, Zhu X and Yang W. NCAPG2 facilitates glioblastoma cells' malignancy and xenograft tumor growth via HBO1 activation by phosphorylation. Cell Tissue Res 2021; 383: 693-706.
[44] Wang S, Li Y, Xing C, Ding C, Zhang H, Chen L, You L, Dai M and Zhao Y. Tumor microenvironment in chemoresistance, metastasis and immunotherapy of pancreatic cancer. Am J Cancer Res 2020; 10: 1937-1953.
[45] Bian J, Lin J, Long J, Yang X, Yang X, Lu X, Sang X and Zhao H. T lymphocytes in hepatocellular carcinoma immune microenvironment: insights into human immunology and immunotherapy. Am J Cancer Res 2020; 10: 4585-4606.

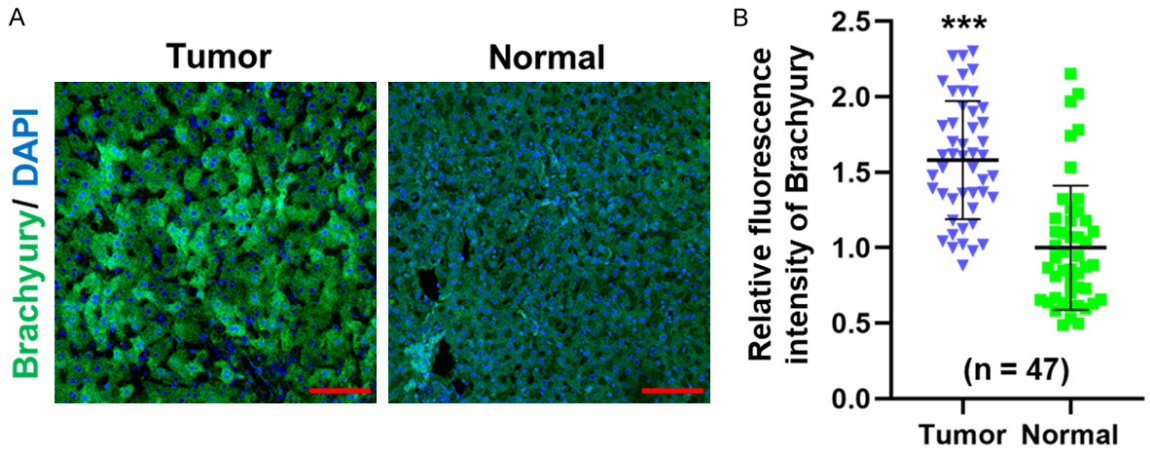

Figure S1. (A) Immunostaining of brachyury in HCC and paired adjacent normal tissues. (B) Quantification of (A). ***P < 0.001. Scale bar = 100 μm.

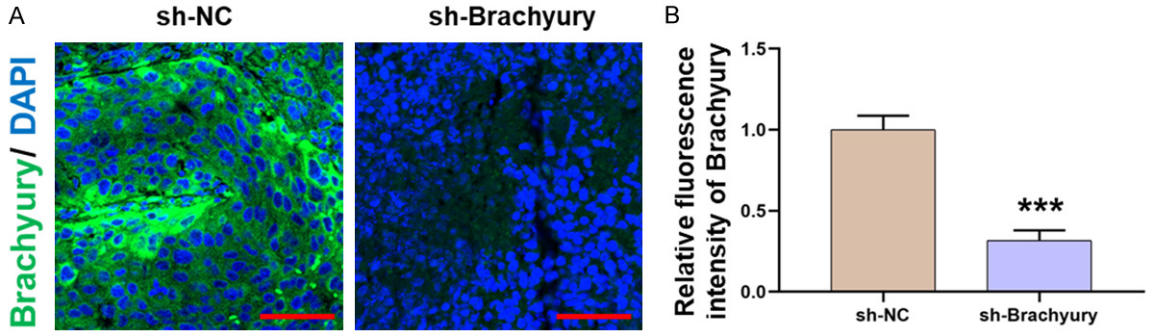

Figure S2. (A) Immunostaining of brachyury in sh-NC and sh-brachyury tumor tissues. (B) Quantification of (A). ***P < 0.001. Scale bar = 50 μm.